Journal of Solid State Chemistry 182 (2009) 966–972

Contents lists available at ScienceDirect

Journal of Solid State Chemistry

journal homepage: www.elsevier.com/locate/jssc

# Two types of carbon nanocomposites: Graphite encapsulated iron nanoparticles and thin carbon nanotubes supported on thick carbon nanotubes, synthesized using PECVD

Guangmin Yang, Xin Wang, Qiang Xu, Shumin Wang, Hongwei Tian, Weitao Zheng *

*Department of Materials Science, State Key Laboratory of Superhard Materials, and Key Laboratory of Automobile Materials of MOE, Jilin University, Changchun 130012, PR China*

ARTICLE INFO

*Article history:*
Received 15 December 2008
Received in revised form
15 January 2009
Accepted 26 January 2009
Available online 5 February 2009

*Keywords:*
Thick CNTs
Encapsulated Fe nanoparticles
Thin CNTs
RF-PECVD

ABSTRACT

In this work, graphite encapsulated Fe nanoparticles and thin carbon nanotubes (CNTs) supported on the pristine CNTs, respectively, were synthesized using plasma enhanced chemical vapor deposition via efficiently controlling the flow rate of discharging $CH_4$ and $H_2$ gas. The properties of the obtained hybrid materials were characterized with superconducting quantum interference and field emission measurements. The results showed that the encapsulated Fe nanoparticles had diameters ranging from 1 to 30 nm, and this hybrid nanocomposite exhibited a ferromagnetic behavior at room temperature. Thin CNTs with an average diameter of 6 nm were attached to the surface of the prepared CNTs, which exhibited a lower turn-on field and higher emission current density than the pristine CNTs. The Fe nanoparticles either encapsulated with graphite or used as catalyst for thin CNTs growth were all originated from the pyrolysis of ferrocene.



## 1. Introduction

Since 1991, there has been extensive research on the synthesis and properties of carbon nanotubes (CNTs) because of their outstanding chemical, electrical and mechanical properties [1]. Due to their nanoscaled and steady structure characteristics and morphologies, as well as inert and resistance properties, CNTs have been considered as ideal supports for metal, inorganic materials, and poly coatings to biomolecules [2–6]. Recent advances in attachment of metal nanoparticles to CNTs provide a way to obtain novel hybrid materials with useful properties for gas sensor, catalytic application, conducting and magnetic materials. For example, metallic nickel, iron, cobalt ferromagnetic nanoparticles are inherently instable in air and acid atmosphere, which limits their potential applications and scientific studies. Therefore, a way to deposit a protective shell, such as silica, organic polymers, or carbon, has been recommended and been researched widely for many years [7–13]. However, to obtain a simple method for preparing carbon encapsulated metallic nanoparticles with controllable size in a high yield is still a significant challenge [14,15]. Very recently, various techniques have been explored to decorate the CNT surface with ferromagnetic nanoparticles to produce metal-CNT composites. Employing thermal evaporation method, Bittencourt et al. have synthesized CNT-Ni composite [16]. Wan et al. [17] have produced magnetic CNT composite by in-situ high-temperature decomposition of the precursor iron (III) acetylacetonate and CNTs in polyol solution. Cheng et al. [18] have concurrently synthesized Ni nanoparticles and carbon encapsulated Ni nanoparticles supported on CNTs using reduction route with CNTs as a reducing agent at 600 °C. The above-mentioned methods have been widely studied for preparing CNT-magnetic nanoparticle composite. However, it turns out that these methods cannot control the intractable agglomeration of the metal nanoparticles. Furthermore, most of the methods are complicated and expensive, and the prepared CNTs randomly distribute in the composite, which is not beneficial to many applications where aligned CNTs on Si substrate are highly desired [19–24]. In this work, using plasma enhanced chemical vapor deposition (PECVD), we explore another method to synthesize aligned CNTs decorated with magnetic Fe nanoparticles encapsulated with graphitic layers. Though the pyrolysis of ferrocene occurs in a mixture of $CH_4$ and $H_2$ atmosphere, the size of Fe nanoparticles can be controlled with a diameter ranging from 1 to 30 nm by changing the deposition time.

On the other hand, a novel hybrid thin–thick CNTs has also been synthesized in this work. After the as-prepared pure CNTs are coated by Fe nanoparticles that are sublimated from the decomposition of ferrocene, subsequent growth of CNTs instead of graphitic layers occur by controlling the flow rate of both discharging $H_2$ and $CH_4$ gas, in which Fe nanoparticles are used as catalyst. We expect that this type of hybrid thin–thick CNTs

* Corresponding author. Fax: +86 431 85168246.
*E-mail address:* WTZheng@jlu.edu.cn (W. Zheng).

0022-4596/$ - see front matter © 2009 Elsevier Inc. All rights reserved.
doi:10.1016/j.jssc.2009.01.036

may have advantages to field electron emissions because the thin CNTs cannot only increase the emission sites but also the field enhancement factors due to their smaller diameters. It should be mentioned that the formation and the enhanced field electron emission property of a similar hybrid material has been already reported by Kim [25], wherein they have synthesized the hybrid multiwall CNTs using consecutive PECVD and thermal CVD growth. PECVD-grown CNTs contain the fragmented catalytic nanoparticles on CNTs' sidewalls. Subsequent thermal CVD growth results in the secondary growth of CNTs on these catalytic nanoparticles. The diameter of about 10 nm for their obtained CNTs from secondary growth is thicker than what we have obtained in this work.

## 2. Experimental

Using magnetron sputtering, we firstly deposited Ti thin film with a thickness of about 30 nm on Si (100) substrate, and then Co thin film with a thickness of about 15 nm as a catalyst for growing CNTs. The synthesis process for growing the hybrid CNTs-graphite encapsulated iron nanoparticles was as follows. Firstly, using two ends of a cylindrical ceramic tube airproofed by steel plates, we made a small hole at the center of one end, and put high-purity ferrocene powders (0.01 g) in the ceramic tube with a diameter of 6 mm. The hole was covered by a piece of Al plate, which was fixed firmly by thin and short aluminum lines around ceramic tube to prevent ferrocene from rapid sublimation. The as-prepared pure CNTs on Si (1 0 0) substrates were placed downstream site in the vapor flow direction at a distance of 4 mm from the ceramic tube. The RF-PECVD reactor chamber was evacuated to a pressure of 8.3 Pa, and the chamber pressure was maintained at 200 Pa with a pure hydrogen (99.99%) gas flow rate of 80 sccm. After the Si substrates was heated to 800 °C for 25 min, the thin aluminum wires in the contacting part of ceramic tube and Al plate were in partially melted and loosed at high temperature (800 °C). About 2 min later, the aluminum plate was partially deviated from the tube end, and Fe atoms sublimated from the ceramic tube (the decomposition of ferrocene had taken place in the zone of the ceramic tube, ferrocene decomposition temperature at about 400 °C) [26] were carried out by discharging $H_2$ gas. Then, the as-prepared pure CNTs were simultaneously coated by the evaporated Fe atoms. Simultaneously, pure methane (99.99%) with a flow rate of 6 sccm was introduced into the chamber for growing hybrid CNTs-graphite encapsulated Fe nanoparticles. During deposition, a radio frequency power of 230 W was applied and the substrate temperature was kept at 800 °C. After 8 or 20 min deposition, $CH_4$ inlet was shut off and the system was allowed to cool down to room temperature.

Different from the deposition for the hybrid CNTs-graphite encapsulated Fe nanoparticles, hybrid thin–thick CNTs were prepared with a $CH_4$ flow rate of 15 sccm and $H_2$ flow rate of 80 sccm. The Fe atoms from the decomposition of ferrocene assembled together to form small particles on the sidewall of as-prepared pure CNTs, and in this case the Fe particles acted as catalyst to grow thin CNTs in discharging $CH_4$ and $H_2$ gas. After 20 min deposition, the $CH_4$ inlet was closed and the system was cooled to room temperature in a $H_2$ atmosphere. The detail experimental parameters are listed in Table 1.

The obtained samples were characterized by scanning electron microscopy (SEM) (JOEL JSM-6700F), transmission electron microscopy (TEM), high resolution transmission electron microscopy (HRTEM) (JOEL JEM-2010 at 300 kV), energy-dispersive X-ray spectroscopy (EDS) (JXA-8200), superconducting quantum interference device (SQUID) magnetometer (MPMS-5S, Quantum Design, San Diego, CA, USA), and field emission measurements.

**Table 1**
Experimental parameters of RF-PECVD.

| Sample | $CH_4$ (sccm) | $H_2$ (sccm) | $T$ (°C) | $P$ (Pa) | Time (min) |
|---|---|---|---|---|---|
| Fig. 1(a) | 80 | 20 | 800 | 1600 | 10 |
| Fig. 1(b) | 6 | 80 | 800 | 1600 | 8 |
| Fig. 1(c) | 6 | 80 | 800 | 1600 | 20 |
| Fig. 4(b) | 15 | 80 | 800 | 1600 | 20 |

TEM and HRTEM samples were prepared by scratching the surface of the obtained sample using a sharp tungsten tip and depositing the collected material on a copper TEM grid. The magnetic properties of the composite films were measured without the Si substrates at room temperature in magnetic fields up to 5 T, using HgCo (NCS) and Ni as standards. The film mass for evaluating the saturation magnetization value was measured using analytical balance (Sartorius BS210S). The field electron emissions for the samples were measured in a parallel plate configuration with an anode-to-sample spacing of 200 μm (using glass fiber as spacers for all experiments). An indium–tin-oxide (ITO) plate was used as an anode to collect the emitted electrons, while nanocarbon films on Si (100) wafer with the size of 1 $cm^2$ were used as the cathode. Prior to measurement, the chamber had been evacuated to a pressure of $1.2 \times 10^{-7}$ Pa through a combined system of turbomolecular pump and ion pump for 60 h, and the samples were heated to degas its surface. During measurement, the pressure in the chamber was maintained at $1.2 \times 10^{-7}$ Pa. As voltage between the electrodes was increased, current flowing to the ITO electrode was recorded.

## 3. Results and discussion

Fig. 1(a) shows a typical SEM image of the morphology for CNTs grown at 800 °C for 10 min, in which the diameter and length of the CNTs are about 10–30 nm and 2.5 μm, respectively. The growth of CNTs has rapidly been accomplished in a short time, about 10 min, and no significant variations in the average diameter and length with prolonging deposition time are observed. Fig. 1(b) and (c) exhibits the morphologies of the CNTs coated with encapsulated Fe nanoparticles, which were produced at 800 °C for 8 and 20 min, respectively, in discharging $H_2$ and $CH_4$ gas. As deposition time is longer, the CNTs are coated more densely bead-shaped nanoparticles. At about 800 °C, a plenty of Fe atoms, decomposed from ferrocene powders, are carried out from the ceramic tube by flowing $H_2$ gas, and are instantly adsorbed on the surface of CNTs. These Fe atoms come together rapidly at high temperature and form nanoparticles. Under the high hydrogen plasma etching, the variation in the distribution density and the size of coated Fe nanoparticles is expected. As the as-prepared Fe-CNT hybrid is exposed to discharging $CH_4$ and $H_2$ gas, most Fe nanopartices are wrapped by graphite layers, which are proved by TEM examinations. The TEM images of the samples are shown in Fig. 2(a) and (b). A number of bead-shaped carbon encapsulated Fe nanoparticles have a radius in the range of 1–30 nm. A HRTEM image in Fig. 2(b-1) and (b-2) shows that the obtained CNTs have a multiple-walled structure (MWCNTs) and carbon encapsulated Fe nanoparticles have an approximately spherical shape. The lattice spacing between adjacent walls of the CNT and the shells of encapsulated Fe nanoparticles has been observed to be 0.34 nm, which is in good agreement with the layer spacing of graphite. The composition of the hybrid CNTs-graphite encapsulated Fe nanoparticles is determined by EDS, and the results are shown in Fig. 2(b-3), in which the presence of C, O, Fe, and Cu are detected. Cu originates from the supporting copper grid, while Fe comes

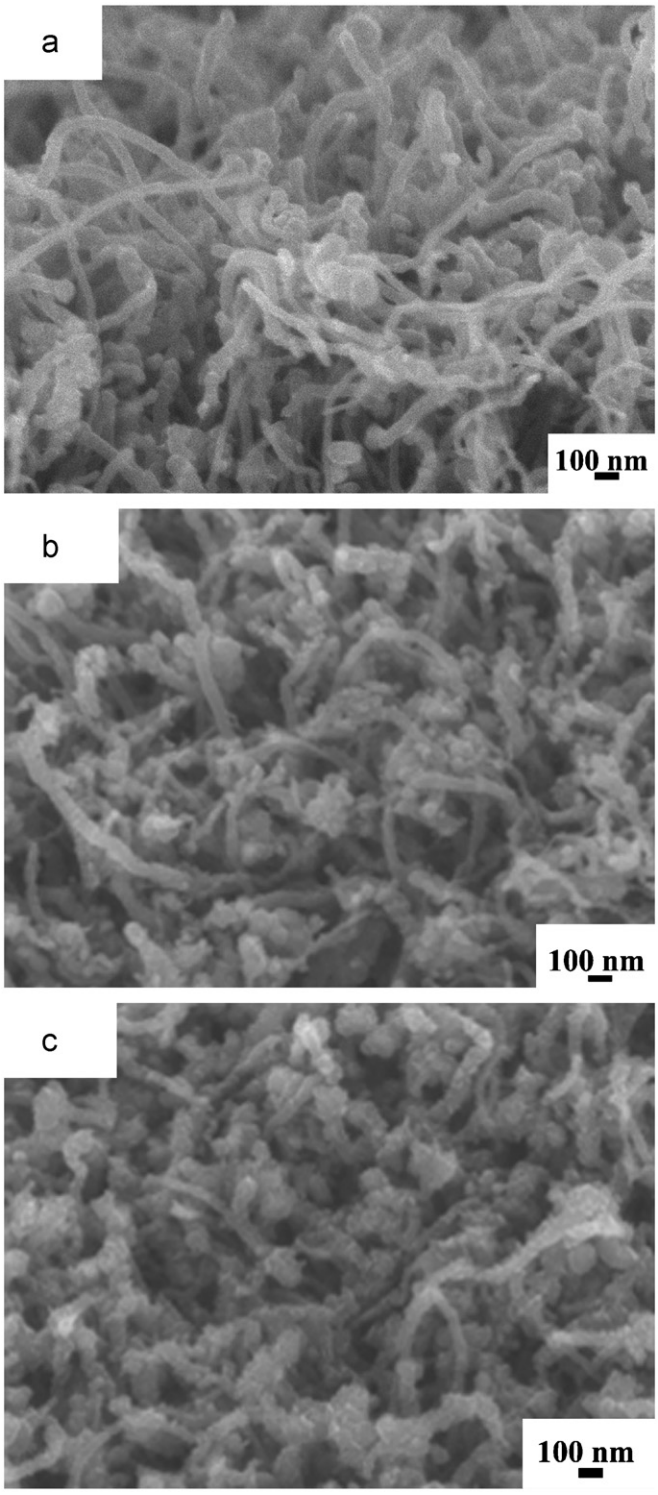


**Fig. 1.** (a) A typical SEM image of pure CNTs grown at 800 °C for 10 min, (b) and (c) SEM images of CNTs-graphite encapsulated Fe nanoparticles at 800 °C grown for 8 and 20 min, respectively.

from ferrocene sublimated. The corresponding selected area electron diffraction pattern (SAED) pattern is displayed in Figs. 2(b-4). The SAED ring pattern can be indexed as a typical BCC structure for Fe, in which the corresponding (110), (200), (211), and (220) Bragg reflections are labeled (see Fig. 2(b-4)), which means that graphite encapsulated Fe nanoparticles have been successfully prepared on CNTs surface.

For comparison, Fig. 3 exhibits the normalized Raman spectra for (a) pure CNTs, (b) CNT-graphite encapsulated Fe nanoparticles grown for 8 min and (c) 20 min, respectively, in which each spectrum shows two characteristic bands, i.e., the disorder graphitic D-band around 1350 $cm^{-1}$ and the G-band around 1580 $cm^{-1}$ that is related to in-plane $sp^2$ vibrations [27–29]. Generally, the intensity ratio of the D over G-band is measured and denoted as the *R*-value: $R = I_D/I_G$, which represents the degree of disorder for the structure of carbonaceous material. In Fig. 3, the hybrid CNT-carbon encapsuled Fe nanoparticles are more disorder than pristine CNTs, which might be the hydrogen plasma etching on the as-prepared CNTs during the pyrolysis of ferrocene.

Fig. 4(a) shows a typical SEM image for pristine CNTs grown at 800 °C, wherein the diameters of CNTs are 15–70 nm and their lengths are about 2 μm. After the as-prepared CNTs are decorated with Fe nanoparticles, the nucleation and growth of thin CNTs around the attached catalyst particles occur. This process results in a secondary growth of random oriented CNTs with much smaller diameters on the sidewalls or tips of the as-prepared CNTs, which look like vines winding around the tree, as shown in Fig. 4(b). Fig. 4(c) is a typical TEM image for the obtained hybrid thin and thick CNTs, in which thin CNTs have diameters about 6 nm, branched out from the as-prepared thick CNTs with a diameter of about 40 nm.

The formation mechanism of the hybrid CNTs-carbon encapsulated Fe nanoparticles can be well explained, based on the vapor–liquid–solid model. At elevated temperature, ferrocene molecules quickly decompose into Fe atoms, which tend to deposit on the sidewalls of the as-prepared CNTs, due to a strong affinity between Fe and C. Because of their small sizes and being dissolved by carbon, the melting points of Fe clusters are far below that of the bulk Fe [30]. It can be deduced that Fe clusters are in a liquid state during the decomposition and may contract to form liquid Fe nanoparticles under surface tension. As the reaction proceeds, some Fe nanoparticles gradually become larger and act as the sites for growing carbon radicals in discharging $CH_4$ and $H_2$ gas. In addition, the etching effect of discharging $H_2$ gas increases the defects on the surface of the formed CNTs [31], which facilitates and stabilizes the decoration of Fe nanoparticles on the MWCNT surface.

As mentioned above, although a variety of nanoparticles ranging from several to tens of nanometers in size have already been synthesized attached to the CNTs surface by wet chemical methods, it is not easy for using wet strategies to obtain an uniform and stable decoration of CNTs with so small Fe nanoparticles as what we have obtained in this work. During deposition, the growth of decorated Fe nanoparticles will be suppressed by plasma etching, and meanwhile the dissolution of carbon into Fe particles should also occur. As the flow rate ratio of $CH_4/H_2$ is small enough to restrain the carbon from supersaturating in Fe nanoparticles, the thicker graphitic layers tend to be accumulated on the surface of the catalytic particles [32]. These particles are energetically favorable for encapsulating themselves into carbon cages. However, whether carbon encapsulating Fe nanoparticles can be formed is dependent on many factors such as experimental parameters and the properties of metallic particles. In this work, what types of the synthesized nanocomposites can be realized are dependent on the carbon concentration in the discharging gases, i.e., the $CH_4$ content in discharging $CH_4$ and $H_2$ gas. As $CH_4$ content increases, the dissolution of the released carbon into the Fe nanoparticles increases. As the $CH_4$ content reaches a critical point, carbon atoms quickly become saturated in the Fe particles due to the carbon solubility limit, and the segregation for carbon atoms occur, which determines the type of final composite product. As the segregation for carbon atoms proceeds, the CNTs grow

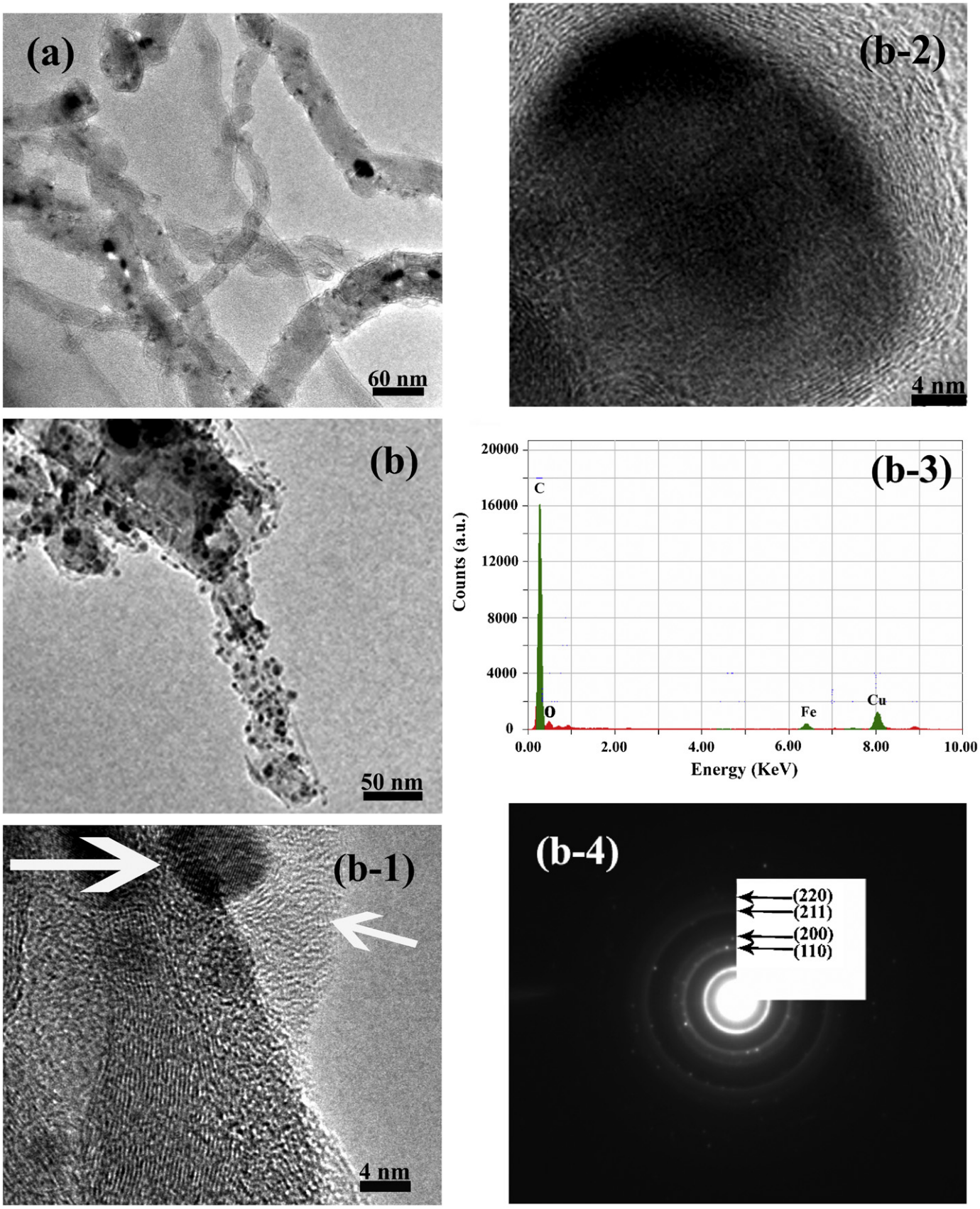


**Fig. 2.** (a) TEM images of CNTs-graphite encapsulated Fe nanoparticles grown for 8 min and (b) 20 min, in which (b-1), (b-2), (b-3), and (b-4) are the corresponding HRTEM images, EDS, and SAED pattern of Fig. 2(b).

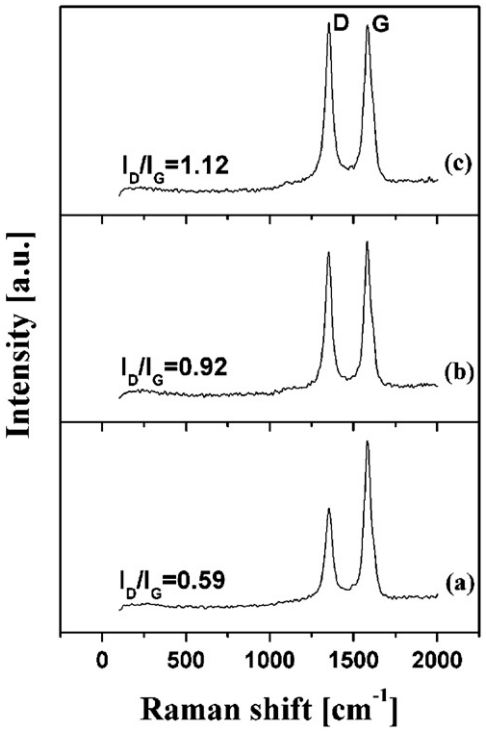


**Fig. 3.** Raman spectra of (a) pure CNTs (curve A) and CNTs-graphite encapsulated Fe nanoparticles grown for 8 and 22 min (curves B and C) in the range of 0–2000 cm$^{-1}$.

continuously [33,34]. In our previous work [35], it has been revealed that three factors including a hydrogen atmosphere, excessive supply of carbon source, and larger size of the catalyst particles play a key role in the growth of CNTs. However, in this work, although the flow rate ratio of $H_2/CH_4$ increases, meaning that the etching from hydrogen plasma irradiation is severe, thin CNTs can also been synthesized. Therefore, as long as enough carbon concentration is provided from $CH_4$, the secondary growth of CNTs can be realized via the formation of small Fe nanoparticles due to severe $H_2$ etching during pyrolysis of ferrocene, since these small Fe nanoparticles are very active and promote the growth of thin CNTs. It should mention that the growth mechanism of both CNTs and graphite encapsulated metal nanoparticles has been reported [36–40], which reveals that the different catalytic activity of metal particles, growth temperatures, and substrates can result in the different products. However, in this work, the flow rate ratio of $CH_4/H_2$ also plays a crucial role in growing both the thin–thick CNTs and CNTs-graphite encapsulated metal nanoparticles composites, since these two types of composites are obtained under almost the same deposition conditions except that the $CH_4$ concentration in discharging $CH_4$ and $H_2$ gas is different.

The magnetization curves of pure CNTs and graphite encapsulated Fe nanoparticles on CNTs are given in Fig. 5, in which the pure CNTs sample, grown using Co nanoparticles as catalyst, has a strong diamagnetic signal from the CNTs, as shown in Fig. 5(a), whereas, in Fig. 5(b), the composite sample exhibits a typical ferromagnetic behavior and the curve is symmetric around $H = 0$. The smooth S-shaped curve has a saturation magnetization ($Ms$) of about 80 emu/g. Considering the small size of Fe nanoparticles decorated on the MWCNT surface, it is expected that a reduction in $Ms$ occurs, compared to bulk Fe ($Ms = 222$ emu/g) [41], due to the coexistence of nonmagnetic carbon and a large surface spin percentage with disordered magnetization orientation for the nanoparticles [42]. Compared to bulk

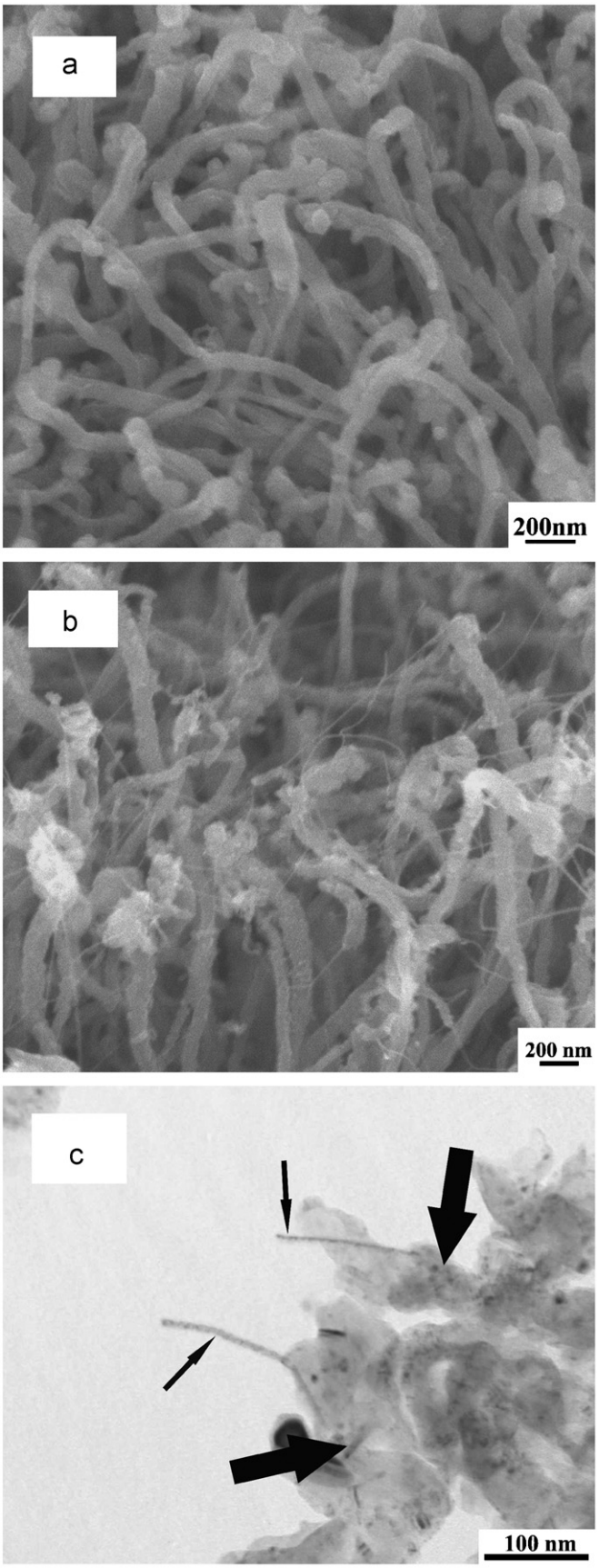


**Fig. 4.** SEM image of (a) pure CNTs and (b) hybrid thin–thick CNTs, and (c) TEM image of hybrid thin–thick CNTs.

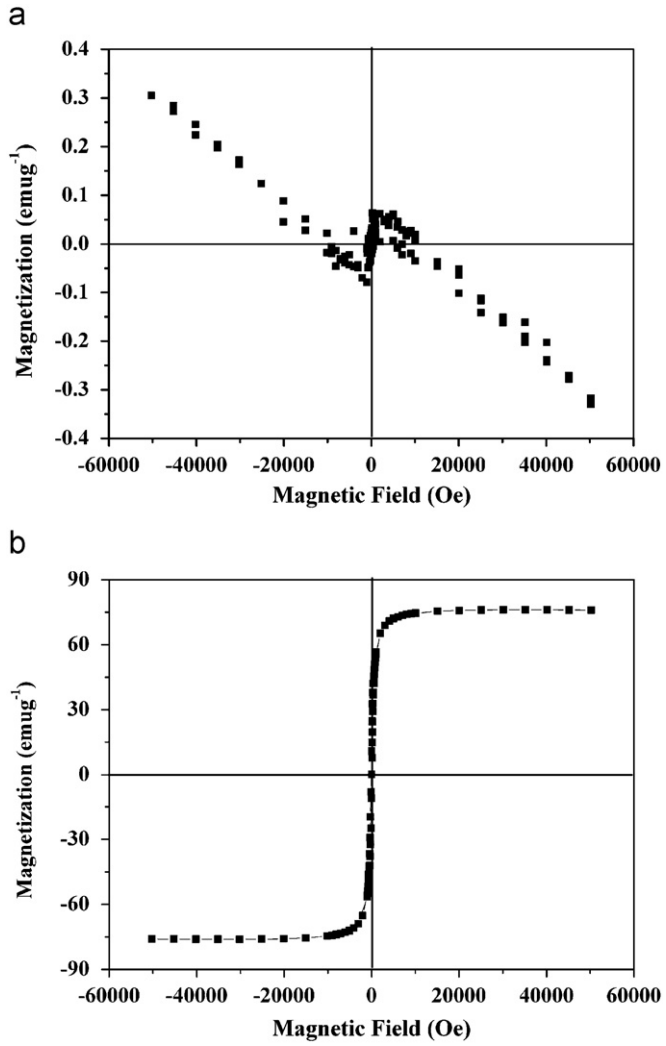


**Fig. 5.** Magnetization curve measured at room temperature for (a) the pure CNTs, (b) CNTs-graphite encapsulated Fe nanoparticles grown for 20 min.

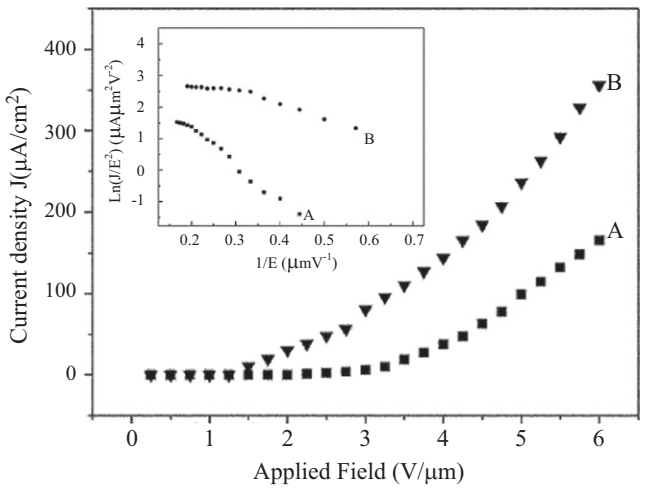


**Fig. 6.** Field emission current density as a function of electric field for (A) the pure CNTs, (B) hybrid thin–thick CNTs, wherein the inset exhibits the Fowler-Nordheim (F-N) plots, corresponding to (A) and (B), respectively.

Fe ($Hc \approx 1$ Oe), an enhancement in coercivity for graphite encapsulated Fe nanoparticles supported on CNTs ($Hc = 60$ Oe) is observed.

Fig. 6 shows the *J*-*E* profiles and Fowler-Nordheim (F-N) plots of the field electron emissions from (A) pure CNTs, (B) hybrid thin–thick CNTs, respectively, in which the turn-on fields (corresponding to an electron emission density of 10 μA/cm$^2$) for as-prepared pure CNTs and hybrid thin–thick CNTs are 3 and 1.3 V/μm, respectively, as shown in Fig. 6. This demonstrates that the hybrid thin–thick CNTs have significantly improved the field electron emission properties, compared to pure CNTs. The inset in Fig. 6 exhibits the corresponding F-N plots ($\ln(J/E^2)$ vs. $1/E$) for pure CNTs and hybrid thin–thick CNTs. The data roughly follows the F-N Eq. (1) in the following, indicating that the field electron emissions for the samples have the mechanism of a quantum mechanical tunneling over a barrier.

$$\ln(J/E^2) = \ln(A\beta^2/\varphi) - B\varphi^{3/2}/\beta E \quad (1)$$

where $A = 1.54 \times 10^{-6}$ AeVV$^{-2}$ and $B = 6.83 \times 10^3$ eV$^{-3/2}$Vμm$^{-1}$ are constants, $\beta$ the field enhancement factor, and $\varphi$ the work function of emitters. Based on the triangular-barrier approximation and the F-N model, using the slope of the F-N plot, $\beta$ of CNTs is calculated to be $6.9 \times 10^3$, whereas that of the hybrid thin–thick CNTs ($\varphi_{CNT} = 5.0$ eV) is estimated to be $1.83 \times 10^4$, indicating that $\beta$ for the hybrid thin–thick CNTs is much higher than that for pure CNTs. This result proves that the hybrid thin–thick CNTs not only have more emission sites, but also enhance $\beta$.

## 4. Conclusions

The hybrid CNTs-graphite encapsulated Fe nanoparticles as well as hybrid thin–thick CNTs can be synthesized via a straightforward method. The small Fe nanoparticles with the size ranging from 1 to 30 nm can be encapsulated with graphitic layers and tightly anchored on the CNTs surface, whereas the secondary growth of CNTs with a diameter of about 6 nm can be catalytically synthesized on Fe nanoparticles residing on the sidewalls of the prepared-CNTs. What types of composites can be obtained are heavily dependent on the flow rate ratio of $CH_4/H_2$. The hybrid CNTs-carbon encapsulated Fe nanoparticles show a ferromagnetic behavior at room temperature, and the hybrid thin–thick CNTs exhibit the enhanced field emission characteristics with a lower turn-on field and higher current density, compared to pristine CNTs. This work demonstrates that the $CH_4$ concentration in discharging $CH_4$ and $H_2$ gas and the size of catalyst particles play a vital role in the growth of either graphite encapsulated Fe nanoparticles or thin carbon nanotubes.

## Acknowledgments

The authors would like to thank the support from National Natural Science Foundation of China (Grant nos. 50832001 and 50525204), the National Key Basic Research and Development Program (Grant no. 2004CB619301), and Project 985—Automotive Engineering of Jilin University.

## References

[1] S. Iijima, Nature 354 (1991) 56.
[2] G.G. Wildgoose, C.E. Banks, R.G. Compton, Small 2 (2006) 182.
[3] M. Baibarac, P. Gómez-Romero, J. Nanosci. Nanotechnol. 6 (2006) 289.
[4] Y. Lin, S. Taylor, H. Li, K.A. Shiral Fernando, L. Qu, W. Wang, L. Gu, B. Zhou, Y.P. Sun, J. Mater. Chem. 14 (2004) 527.
[5] M. Burghard, K. Balasubramanian, Small (2005) 180.
[6] J. Chen, H. Liu, W.A. Weimer, M.D. Halls, D.H. Waldeck, G.C. Walker, J. Am. Chem. Soc. 124 (2002) 9034.
[7] U. Jeong, X. Tneg, Y. Wang, H. Yang, Y. Xia, Adv. Mater. 19 (2007) 33.
[8] N. Junichi, O. Chie, O. Osamu, N. Nobuyuki, Carbon 44 (2006) 2943.
[9] G.X. Zhu, X.W. Wei, C.J. Xia, Y. Ye, Carbon 45 (2007) 1160.

[10] R. Seshadri, R. Sen, G.N. Subbanna, K.R. Kannan, C.N.R. Rao, Chem. Phys. Lett. 231 (1994) 308.
[11] X.C. Sun, X.L. Dong, Mater. Res. Bull. 37 (2002) 991.
[12] Y.W. Ma, Z. Hu, L.S. Yu, Y.M. Hu, B. Yue, et al., J. Phys. Chem. B 110 (2006) 20118.
[13] Q.F. Liu, W.C. Ren, Z.G. Chen, B.I. Liu, B. Yu, F. Li, H.T. Cong, H.M. Cheng, Carbon 46 (2008) 1417.
[14] S.W. Liu, J.J. Zhu, Y. Mastai, I. Felner, A. Gedanken, Chem. Mater. 12 (2000) 2205.
[15] X.K. Li, Z.X. Lei, R.C. Ren, J. Liu, X.H. Zuo, Z.J. Dong, H.Z. Wang, J.B. Wang, Carbon 41 (2003) 3068.
[16] C. Bittencourt, A. Felten, J. Ghijsen, J.J. Pireaux, W. Drube, R. Erni, G. Van Tendeloo, Chem. Phys. Lett. 436 (2007) 368.
[17] J.Q. Wan, W. Cai, J.T. Feng, X.X. Meng, E.Z. Liu, J. Mater. Chem. 17 (2007) 1188.
[18] J.P. Cheng, X.B. Zhang, Y. Ye, J. Solid State Chem. 179 (2006) 91.
[19] S.S. Fan, M.G. Chapline, N.R. Franklin, T.W. Tombler, A.M. Cassell, H.J. Dai, Science 283 (1999) 512.
[20] A. Patil, T. Ohashi, A. Buldum, L.M. Dai, Appl. Phys. Lett. 89 (2006) 103103.
[21] H. Murakami, M. Hirakawa, C. Tanaka, H. Yamakawa, Appl. Phys. Lett. 76 (2000) 1776.
[22] Q.L. Chen, K.H. Xue, W. Shen, F.F. Tao, S.Y. Yin, W. Xu, Electrochim. Acta 49 (2004) 4157.
[23] M. Arab, F. Berger, F. Picaud, C. Ramseyer, J. Glory, M. Mayne-L'Hermite, Chem. Phys. Lett. 433 (2006) 175.
[24] J.Y. Li, Y.F. Zhang, Physica E 33 (2006) 235.
[25] H.J. Kim, I.T. Han, Y. Jun Park, J.M. Kim, J.B. Park, B.K. Kim, N.S. Lee, Chem. Phys. Lett. 396 (2004) 6.
[26] B.Y. Liu, D.C. Jia, Q.C. Meng, J.C. Rao, Carbon 45 (2007) 668.
[27] A. Malesevic, S. Vizireanu, R. Kemps, A. Vanhulsel, C. Van Haesendonck, G. Dinescu, Carbon 45 (2007) 2932.
[28] E.T. Thostenson, W.Z. Li, D.Z. Wang, Z.F. Ren, T.W. Chou, J. Appl. Phys. 91 (9) (2002) 6034.
[29] Q.T. Li, Z.C. Ni, J.L. Gong, D.Z. Zhu, Z.Y. Zhu, Carbon 46 (2008) 434.
[30] M.H. Rummeli, E. Borowiak-Palen, T. Gemming, T. Pichler, M. Knupfer, M. Kalbac, et al., Nano. Lett. 5 (7) (2005) 1209.
[31] S. Trasobares, C.P. Ewels, J. Birrell, O. Stephan Bingqing, Q. Wei, J.A. Carlisle, D. Miller, P. Keblinski, P.M. Ajayan, Adv. Mater. 16 (2004) 670.
[32] J. Jiao, S. Seraphin, J. Phys. Chem. Solids 61 (2000) 1055.
[33] W.Z. Li, S.S. Xie, L.X. Qian, B.H. Chang, B.S. Zou, W.Y. Zhou, Science 274 (1996) 1701.
[34] M. Meyyappan, L. Delzeit, A. Cassell, D. Hash, Plasma Sources Sci. Technol. 12 (2003) 205.
[35] J.W. Liu, X. Wang, W.T. Zheng, J.X. Li, Q.F. Guan, Y.D. Su, J.L. Qi, Q. Jiang, Carbon 45 (2007) 668.
[36] C.N. He, N.Q. Zhao, C.S. Shi, X.W. Du, J.J. Li, Mater. Chem. Phys. 97 (2006) 109.
[37] J.L. Kang, J.J. Li, X.W. Du, C.S. Shi, N.Q. Zhao, P.L. Nash, Mater. Sci. Eng. A (2007).
[38] N. Sano, H. Akazawa, T. Kikuchi, T. Kanki, Carbon 41 (2003) 2159.
[39] B.H. Liu, J. Ding, Z.Y. Zhong, Z.L. Dong, T. White, J.Y. Lin, Chem. Phys. Lett. 358 (2002) 96.
[40] A.G. Nasibulin, A. Moisala, D.P. Brown, E.I. Kauppinen, Carbon 41 (2003) 2711.
[41] S.I. Nikitenko, Y. Koltypin, O. Palchik, I. Felner, X.N. Xu, A. Gedanken, Angew. Chem. Int. Ed. 40 (2001) 404447.
[42] K. Lafdi, A. Chin, N. Ali, J.F. Despres, J. Appl. Phys. 79 (1996) 6007.